JOURNAL OF COMPUTATIONAL PHYSICS 10, 487–502 (1972)

A Computational Method for Low Mach Number Unsteady Compressible Free Convective Flows

C. K. FORESTER

The Boeing Company, Seattle, Washington 98124

AND

A. F. EMERY

Department of Mechanical Engineering, University of Washington, Seattle, Washington, and Sandia Laboratories, Livermore, California 98125

Received April 13, 1972

The General Elliptic Method (GEM) for computing time-dependent, two-dimensional, compressible, free convection flows at low Mach number is presented. The principal feature of the GEM algorithm is the manner in which the average fluid pressure and the local fluid density are varied. Sample calculations of incompressible and compressible free convection flows are presented.

INTRODUCTION

It is usual to consider low Mach number free convection flows as incompressible with the density variation effects confined to the buoyancy terms in the momentum equations. However, for free convection flow for which the density variations are large, this assumption, the classical Boussinesq assumption [1], may not provide a basis which is sufficiently accurate. This is particularly true when the temperature variations are sufficient to require the consideration of variable properties.

In this paper we wish to show that the Boussinesq assumption need not be employed and that the MAC method developed by Harlow and Welch [2] for simulating incompressible fluid flow with free surfaces can be extended to compressible free convection problems by incorporating thermal and pressure expansion effects. Within the accuracy of the finite difference approximations, this approach provides a consistent treatment of the problem according to Mihaljan's

definitions. This computational procedure will be called the General Elliptic Method (GEM).

The GEM algorithm utilizes the usual centered difference expressions for the pressure gradient, buoyant, viscous, and heat conduction terms with forward differences for the time derivatives. For the test calculations, donor cell and centered difference expressions for the advective terms have been used. For the simulation of inviscid adiabatic flow, these difference approximations substantially damp or amplify (respectively) the kinetic energy of a region of interest and therefore for these flows they are particularly poor approximations. Additionally, these difference approximations exhibit poor dispersive properties (see Fromm [7]). Williams [16], Crowley [17], and Fromm [18], to name a few, have made progress in developing improved advective schemes. With these results for encouragement, it is not unreasonable to believe that the GEM algorithm can be modified to include improved advective approximations. However, in the type of free convection flows of interest here, the viscous, buoyant, and pressure gradient terms dominate the momentum advection terms with the result that the choice which is made for approximating these latter terms is not critical. This is confirmed both with numerical convergence studies and with physical experiments. In the latter, measured velocity and temperature profiles and overall heat transfer rates have been found to be in good agreement with the predictions using first order advective schemes [3, 4]. Recently the GEM algorithm has been extended to include the effects of elastic container walls and has been used to successfully predict some of the pressure and temperature fluctuations which have been observed in the single-phase cryogenic oxygen storage systems of the Apollo spacecraft [5, 19].

Formulation of the Difference Equations

The appropriate differential equations for the subsonic flow of a Newtonian fluid subject to the restrictions

a. Two-dimensional flow

b. Absence of viscous dissipation and acoustic waves

c. Kinetic energy contribution to the internal energy is assumed to be zero

d. Lack of potential forces (e.g., surface tension, solid–fluid attraction)

e. Fluid properties which are independent of dynamic effects (e.g., the thermal conductivity is not dependent upon the temperature gradient)

f. No radiant energy exhange (this restriction is not formally necessary but is involved in order to simplify the methodological presentation)

are

$$\frac{\partial \rho}{\partial t} + \frac{\partial \rho u}{\partial x} + \frac{\partial \rho v}{\partial y} = 0, \tag{1a}$$

$$\frac{\partial \rho e}{\partial t} + \frac{\partial \rho u h}{\partial x} + \frac{\partial \rho v h}{\partial y} = \frac{\partial}{\partial x}\left(k \frac{\partial T}{\partial x}\right) + \frac{\partial}{\partial y}\left(k \frac{\partial T}{\partial y}\right), \tag{1b}$$

$$\frac{\partial \rho u}{\partial t} + \frac{\partial \rho u^2}{\partial x} + \frac{\partial \rho u v}{\partial y} + \frac{\partial P}{\partial x} + g_x \rho = \sigma_x, \tag{1c}$$

$$\frac{\partial \rho v}{\partial t} + \frac{\partial \rho u v}{\partial x} + \frac{\partial \rho v^2}{\partial y} + \frac{\partial P}{\partial y} + g_y \rho = \sigma_y, \tag{1d}$$

where for illustrative purposes we employ Stoke's relation to give

$$\sigma_x = \frac{\partial}{\partial x}\left\{2\mu \frac{\partial u}{\partial x} - \frac{2}{3}\mu\left(\frac{\partial u}{\partial x} + \frac{\partial v}{\partial y}\right)\right\} + \frac{\partial}{\partial y}\left\{\mu\left(\frac{\partial u}{\partial y} + \frac{\partial v}{\partial x}\right)\right\},$$

$$\sigma_y = \frac{\partial}{\partial y}\left\{2\mu \frac{\partial v}{\partial y} - \frac{2}{3}\mu\left(\frac{\partial u}{\partial x} + \frac{\partial v}{\partial y}\right)\right\} + \frac{\partial}{\partial x}\left\{\mu\left(\frac{\partial u}{\partial y} + \frac{\partial v}{\partial x}\right)\right\}.$$

From the relation

$$-T\,ds = de + \frac{P}{\rho^2}\,d\rho = \frac{\partial e}{\partial \rho}\bigg|_p d\rho + \frac{\partial e}{\partial P}\bigg|_\rho dP + \frac{P}{\rho^2}\,d\rho = \frac{\partial h}{\partial \rho}\bigg|_p d\rho + \frac{\partial e}{\partial P}\bigg|_\rho dP, \tag{2a}$$

we define two fluid properties θ and ϕ as

$$\theta \equiv -\rho \frac{\partial h}{\partial \rho}\bigg|_p = \frac{c_P}{\beta}, \qquad \phi \equiv \frac{1}{\rho}\frac{\partial P}{\partial e}\bigg|_\rho = \frac{1}{\rho}\frac{\beta}{\kappa c_v}, \tag{2b}$$

whose product $\theta\phi$ is the speed of sound squared. The mass fluxes $\overline{X}$ and $\overline{Y}$ through the sides of a cell enclosing a nodal point are defined as

$$\overline{X} \equiv \rho u A_x, \qquad \overline{Y} \equiv \rho v A_y \tag{3}$$

(A_x and A_y are the constant areas of the cell sides perpendicular to the x and y axes, respectively), Equations (1a) and (1b) can be written for rectangular grids as

$$\frac{\partial \rho}{\partial t} + \frac{1}{A_x}\frac{\partial \overline{X}}{\partial x} + \frac{1}{A_y}\frac{\partial \overline{Y}}{\partial y} = 0, \tag{4a}$$

$$\begin{aligned}\frac{dP_a}{dt} = &+ \phi\left\{\frac{\partial}{\partial x}\left(kA_x \frac{\partial T}{\partial x}\right) - \overline{X}\frac{\partial h}{\partial x}\right\}\Big/A_x \\ &+ \phi\left\{\frac{\partial}{\partial y}\left(kA_y \frac{\partial T}{\partial y}\right) - \overline{Y}\frac{\partial h}{\partial y}\right\}\Big/A_x \\ &- \phi\theta\left\{\frac{1}{A_x}\frac{\partial \overline{X}}{\partial x} + \frac{1}{A_y}\frac{\partial \overline{Y}}{\partial y}\right\}.\end{aligned} \tag{4b}$$

The energy equation, Eq. (4b), is expressed in terms of the pressure rather than the internal energy. Because of assumptions b and c— the absence of acoustic waves and kinetic energy—the time rate of change of the pressure has been taken to be independent of the spatial coordinates. The replacement of the local pressure by the average fluid pressure takes place only in the compression work term for the energy equation and not in the momentum equations and therefore the algorithm is restricted to flows in which dynamic compressive or expansive pressure effects are negligible (i.e., Mach number and Eckert numbers are small). Since the left hand side of Eq. (4b) is taken to be independent of position, this equation will force a special relationship between D_{ij} of any cell and the net energy influx E_{ij} into that cell [see Eq. (6a)]. Equation (4b) will not locally conserve energy unless special procedures are used to time center the speed of sound squared ($\phi\theta$) and θ except in the case of ideal gases for which $\theta = h$ and $\phi = R/c_v$, a constant.

For most pure substances, θ and ϕ are nearly constant with respect to the density, even near the critical point. As the fluid deviates from the critical point, θ varies more strongly than ϕ, but both are well-behaved functions of ρ in both the single-phase region and in the two-phase region near the critical point.

Equations (1c) and (1d) may be expressed as

$$\frac{\partial \overline{X}}{\partial t} + \frac{\partial(u\overline{X})}{\partial x} + \frac{A_x}{A_y}\frac{\partial(u\overline{Y})}{\partial y} = -A_x\frac{\partial P}{\partial x} + A_x(\sigma_x - \rho g_x), \tag{4c}$$

$$\frac{\partial \overline{Y}}{\partial t} + \frac{A_y}{A_x}\frac{\partial(v\overline{X})}{\partial x} + \frac{\partial(v\overline{Y})}{\partial y} = -A_y\frac{\partial P}{\partial y} + A_y(\sigma_y - \rho g_y). \tag{4d}$$

Finite Difference Formulation

Since the type of difference expressions which are used for the viscous, buoyant, and advection terms are not unusual, these expressions are omitted in the following text but may be found in complete form in Ref. [8].

The difference forms of Eqs. (4a)–(4d) for a uniform two-dimensional rectangular grid with a unit depth in the third dimension are

$$\rho_{ij}^{n+1} = \rho_{ij}^{n} + D_{ij}^{n+1}\frac{\Delta t}{V}, \tag{5a}$$

$$P_a^{n+1} = P_a{}^n + \phi_{ij}^{n+\delta}\left[E_{ij}^{n+\delta} + \theta_{ij}^{n+\delta}D_{ij}^{n+1}\right]\frac{\Delta t}{V}, \tag{5b}$$

$$\overline{X}_{i+1/2j}^{n+1} = \overline{X}_{i+1/2j}^{n} + A_x\left[\frac{(P_{ij} - P_{i+1j})^{n+1}}{\Delta x} + HX_{i+1/2j}^{n}\right]\Delta t, \tag{5c}$$

$$\overline{Y}_{ij+1/2}^{n+1} = \overline{Y}_{ij+1/2}^{n} + A_y\left[\frac{(P_{ij} - P_{ij+1})^{n+1}}{\Delta y} + HY_{ij+1/2}^{n}\right]\Delta t, \tag{5d}$$

where

$$D_{ij}^{n+1} = (\bar{X}_{i-1/2j} - \bar{X}_{i+1/2j} + \bar{Y}_{ij-1/2} - \bar{Y}_{ij+1/2})^{n+1},$$

and

$$V = A_x \Delta x = A_y \Delta y,$$

and the superscripts $n + 1$ and $n + \delta$ indicate an evaluation at the time $(n + 1)\,\Delta t$ or $(n + \delta)\,\Delta t(\delta \leqslant 1)$, respectively.

D_{ij} and E_{ij} are the net mass rate and energy rate (by conduction and advection) to the ij cell, respectively, while HX and HY represent the sum of the body force, the viscous forces, and the momentum advection terms in the x and y directions, respectively. The body forces may be evaluated at $t + \Delta t$ or at $t + \Delta t/2$ although the numerical tests indicate that the latter evaluation yields improved stability.

To use GEM, Eq. (5b) is written as

$$D_{ij}^{n+1} = \dot{P}_a \left(\frac{V}{\phi\theta}\right)_{ij}^{n+\delta} - \left(\frac{E}{\theta}\right)_{ij}^{n+\delta} \tag{6a}$$

where

$$\dot{P}_a = \frac{P_a^{n+1} - P_a{}^n}{\Delta t}. \tag{6b}$$

Since D_{ij}, when summed over the entire computational region, is equal to the net inflow of mass at the boundaries and since $\dot{P}_a$ is assumed to be spatially constant, Eq. (6a) can be integrated over the fluid region to give

$$\dot{P}_a = \left\{\sum \left(\frac{E}{\theta}\right)_{ij}^{n+\delta} + \begin{matrix}\text{net boundary} \\ \text{inflow}\end{matrix}\right\} \Big/ \sum \left(\frac{V}{\phi\theta}\right)_{ij}^{n+\delta}. \tag{7}$$

Combining Eq. (5a) and (6a),

$$\rho_{ij}^{n+1} = \rho_{ij}^{n} + \left[\dot{P}_a \left(\frac{V}{\phi\theta}\right)_{ij}^{n+\delta} - \left(\frac{E}{\theta}\right)_{ij}^{n+\delta}\right] \frac{\Delta t}{V}. \tag{8}$$

Equations (7) and (8) are the discrete conservation equations of energy and mass which must be solved simultaneously with the momentum equations, Eqs. (5c) and (5d). To do this, we difference the momentum equations and combine them to eliminate $\bar{X}^{n+1}$ and $\bar{Y}^{n+1}$ yielding

$$D_{ij}^{n+1} = D_{ij}^{n} + \Delta t(PXY_{ij}^{n+1} - HXY_{ij}^{n}), \tag{9}$$

where

$$PXY_{ij}^{n+1} = \frac{A_x}{\Delta x}(P_{i-1j} - 2P_{ij} + P_{i+1j})^{n+1} + \frac{A_y}{\Delta y}(P_{ij-1} - 2P_{ij} + P_{ij+1})^{n+1},$$

$$HXY = (HX_{i-1/2j} - HX_{i+1/2j} + HY_{ij-1/2} - HY_{ij+1/2})^n.$$

Combining Eqs. (6) and (9) we finally have

$$PXY_{ij}^{n+1} = \frac{1}{\Delta t}\left\{\dot{P}_a\left(\frac{V}{\phi\theta}\right)_{ij}^{n+\delta} - \left(\frac{E}{\theta}\right)_{ij}^{n+\delta} - D_{ij}^n\right\} + HXY_{ij}^n. \tag{10}$$

Equation (10) is an elliptic difference equation which can be solved by direct inversion, direct Fourier methods [9], or by iteration methods. For ease of handling the considered boundary shapes and simplicity of coding the text problems, the successive over-relaxation method was chosen for the examples treated herein.

If we define NIP as the number of iterations of Eq. (10) and NIE as the number of times that $\dot{P}_a$, ϕ, θ, and E are re-evaluated during each time step, the solution procedure for GEM is:

1. Prescribe initial values of $\overline{X}$, $\overline{Y}$, P_a and ρ
2. Compute u and v from $\overline{X}$ and $\overline{Y}$ and ρ
3. Evaluate T, h, k, μ, $(\phi\theta)$ and θ with P_a and ρ from the thermodynamic tables and transport relations
4. Evaluate HX, HY, D, and E
5. Compute $\dot{P}_a$ and ρ^{n+1} from Eqs. (7) and (8), respectively
6. 6. Re-evaluate $(\phi\theta)$, θ, h, and E at the average of the initial and current values of P_a and ρ
7. Repeat steps 5 and 6 zero, one, or two times. The optimum number must be determined from numerical experiments.
8. Obtain a solution of Eq. (10) and use the resultant values of the cell pressures P_{ij} in the momentum balances (5c) and (5d) to obtain new values of $\overline{X}$ and $\overline{Y}$.
9. Use these values of mass fluxes in E and repeat 5, 6, 7, and 8 NIE times. The optimum number must be determined from numerical experiments.
10. The latest values of $\overline{X}$, $\overline{Y}$, P_{ij}, and P_a may be used to compute a new time cycle from Steps 2–9.

For an ideal gas, Steps 6, 7, and 9 may be omitted since energy is algebraically conserved for such a fluid. However, for general fluids, Steps 5–8 must be repeated NIE times in order to conserve energy to the degree desired. An example of the

importance of this latter consideration for cryogenic oxygen has been presented in Ref. [6]. In this example, nonisothermal cryogenic single-phase oxygen which is adiabatically restored to the isothermal state may exhibit associated pressure decays of hundreds of pounds per square inch. Application of the GEM algorithm to this problem gives rise to errors in the predicted pressure decay which is related to the time step and the value of NIE used. If NIE is zero and the time step is near the maximum allowable value, errors in the predicted adiabatic pressure decay may be in excess of 100%. Fortunately, values of NIE of two or four will hold the error in the predicted adiabatic pressure decay to less than 2% and 0.5%, respectively.

All of the calculations which are reported herein for an ideal gas were made using NIE equal to zero. Stability and energy conservation studies for an ideal gas have been made with NIE equal to zero, two, four, and eight. A significant improvement in the stability properties is obtained for NIE greater than or equal to two.

Stability Considerations

The stability limits of GEM were established by using the positive coefficient rule of Barakat [10] rather than the heuristic approach of Hirt [11] or the Fourier method of von Neumann [12] since the first was found to be the most conservative.

Substituting for $\dot{P}$ in Eq. (1b) using Eq. (4b), the stability criteria for the donor cell differencing of the advection terms gives

$$\frac{1}{\Delta t} \geqslant 2A\left(\frac{C_1}{\Delta x^2}+\frac{C_2}{\Delta y^2}\right)(1+\phi C_3)+\frac{(1+\phi C_4)}{\rho V}\{|\,\overline{X}_{i-1/2j}\,|+|\,\overline{X}_{i+1/2j}\,| + |\,\overline{Y}_{ij-1/2}\,|+|\,\overline{Y}_{ij+1/2}\,|\}\,C_5\,, \tag{11}$$

$$A = \max(k/\rho c_p\,,\ \mu/\rho)_{ij}\,.$$

The constants C_1 and C_2 are unity for cells in the interior of the region and one plus the number of heated cell faces in the x and y directions, respectively, for cells with prescribed heat fluxes. The constants C_3, C_4, and C_5 are zero, $-1/2$, and $1/2$, respectively, for incompressible flow. For compressible flow, C_3 and C_4 are unity and C_5 was found to be between $0.5/(1+\phi)$ and 1; the first value applies when the advective energy terms in Eq. (10) are evaluated at $\delta = 1/2$ with NIE greater than or equal to 2 and the second value applies when δ and NIE are zero.

When the advection terms are center differenced, $1+\phi C_4$ is replaced by $0.5(1+\phi C_4)$ and two additional constraints exist:

$$|\,u\,|_{ij} \leqslant \frac{2A}{\Delta x}\,; \qquad |\,v\,|_{ij} \leqslant \frac{2A}{\Delta y}\,. \tag{12}$$

Numerical tests for $10^3 \leqslant Ra \leqslant 10^9$ substantiated Eq. (11) but suggested that the centered difference limit, Eq. (12), was often too restrictive. It was also observed that sudden changes in the body force caused by step changes in g required that Eq. (11) be re-evaluated after the end of each time step. If Eq. (11) is violated, then that time cycle must be repeated until it is satisfied. However, this costly procedure can be avoided by constraining Δt by

$$\Delta t \leqslant (\max(\Delta x, \Delta y)/2\Delta g)^{1/2} \tag{13}$$

which can be obtained from a similar stability analysis.

Boundary Treatment

Some discussion is now devoted to the various boundary conditions which are required to define all derivatives and quantities normal to the boundary. In order to apply Eqs. (5c), (5d), (6b), (7), (8), and (10) to a physical problem, the volume of interest is divided into a desired number of control volumes or cells. For convenience, it is useful to define a set of fictitious cells adjoining but outside the volume of interest. These cells are used to represent supplier or receiver reservoirs of mass or energy and may be used to establish the appropriate boundary conditions: the alternative to using the fictitious exterior set of cells is to set up special forms of the equations at the boundaries which include the apropriate boundary conditions. For the calculations over a rectangular region of interest, the fictitious cell method of treating the boundary conditions is preferred because it is the simplest to implement.

All mass rates normal to the border must be set to zero except where expulsion or mass injection are specified. Where mass injection is prescribed, the enthalpy and density must be set to some desired value in the fictitious supplier cell. Where mass expulsion is specified, the enthalpy and density of the fictitious receiver cell is set equal to that of the supplier cell. The enthalpies are used in the energy advection terms while the densities are used in the velocity calculations which are normal to and on the border. This velocity enters into two viscous terms. Two other viscous terms require the prescription of velocities parallel to the boundary in all external cells. Where no-slip boundaries are required, the external velocity is set equal and opposite to the values in the active adjoining cell. Where free-slip boundary velocities are required, the external velocity is set equal to the values in the active adjoining cell. These velocities in external cells are computed *after* all the velocities have been computed which reside inside and on the border. The $HX_{i+1/2j}$ and $HY_{ij+1/2}$ terms required by the momentum balances on the border may be set to any value but for convenience are set to zero. This follows from the fact that

since the mass rates at $n + 1$ and n are prescribed on the border, the momentum balances are not required to generate these values at the border. For these to balance then it is only necessary that the values of $HX_{i+1/2j}$ and $HY_{ij+1/2}$ defined on the border which are used in the elliptic Eq. (6) be the same as those used in the border momentum balances to find the unknown external cell pressure which is required by Eq. (6) during the iterative solution.

Exterior cell temperatures are determined from the specified heat flux or from the relation for a left cell face of

$$T_{I-1j} = 8/3T_{Wall} - 2T_{ij} + 1/3T_{I+1j},$$

where T_{Wall} is the prescribed wall temperature and I represents the wall node.

Cavity Flows with Small Density Variations

A two-dimensional region (Fig. 1) is initially filled with a quiescent ideal gas at 560°R. At time zero the left and right hand vertical surfaces are changed to 570°R and 550°R and maintained at these values thereafter. Both top and bottom surfaces are insulated. MacGregor [13], Wilkes [14], and deVahl Davis [15] have previously

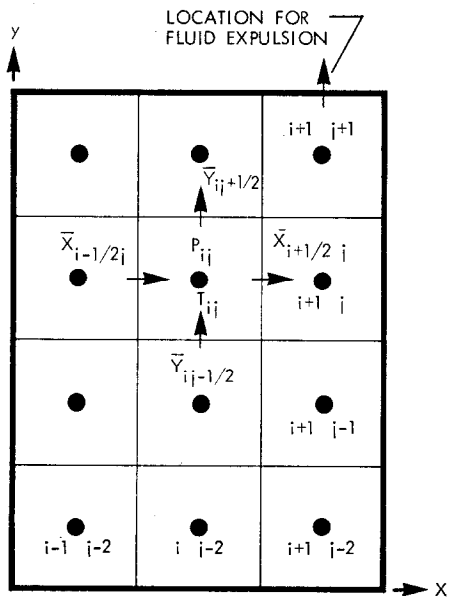

FIG. 1. Physical grid.

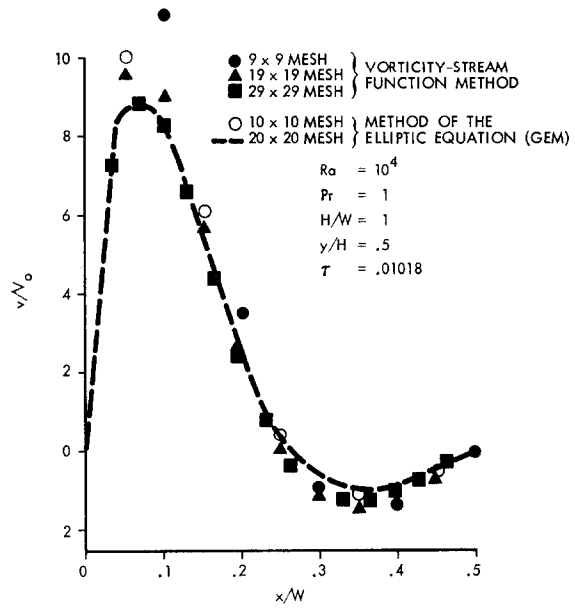

FIG. 2. Incompressible fluid transient velocity profile in a cavity. ($V_0 = \mu/\rho/W$)

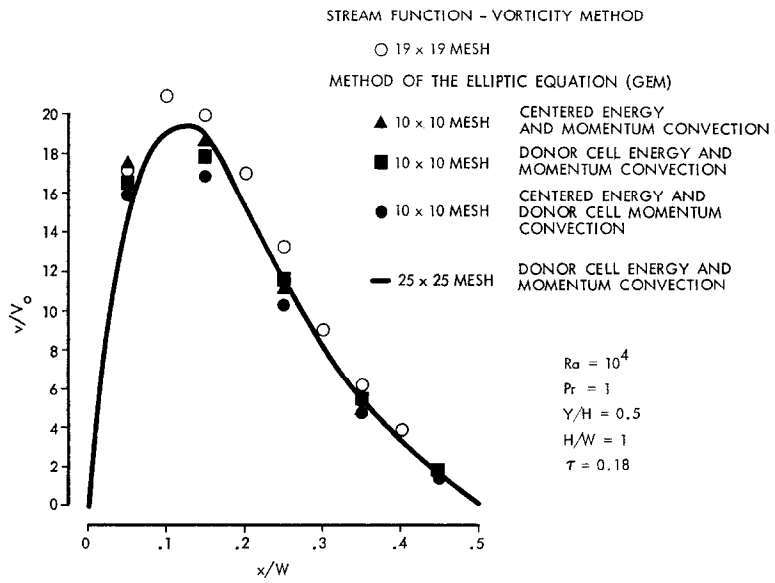

FIG. 3. Incompressible fluid steady state velocity profile in a cavity. ($V_0 = \mu/\rho/W$)

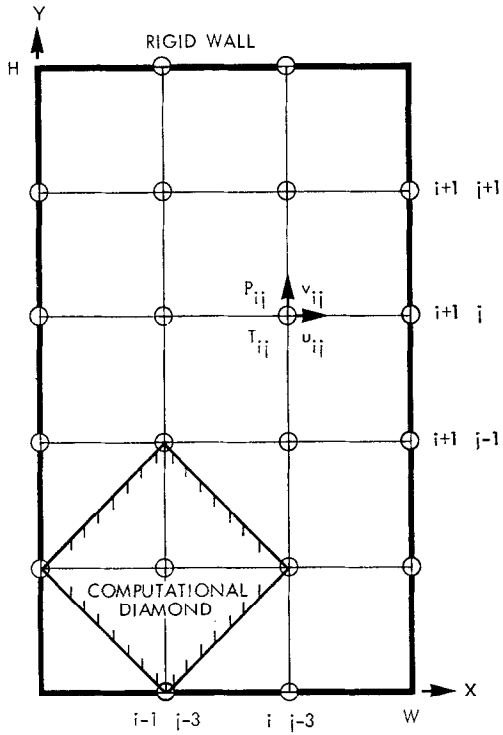

FIG. 4. Mathematical grid.

treated this problem by using the stream-function vorticity formulation to eliminate the hydrostatic pressure in conjunction with the Boussinesq assumption of constant density, except in the body force term. In addition, MacGregor experimentally measured temperature profiles and heat transfer and found good agreement with his first order numerical predictions. Figures 2 and 3 give a comparison of the values of v/V_0 at the mid-height of the cell computed by using GEM and those of MacGregor for an early transient phase and the final steady state. Both methods appear to converge to the same results as the number of mesh points increases. However, the rate of convergence for GEM is higher since the physical grid (Fig. 1) is employed rather than the mathematical grid (Fig. 4) which MacGregor used. It may also be noted in Fig. 3 that the centered difference approximation for the advection of energy and momentum does not provide superior accuracy compared to the donor cell differencing. This result may be interpreted to imply that the degree of damping or amplification of kinetic energy inherent in the donor cell or centered difference methods of momentum advection, respectively, are not important for free convection flow where the pressure, bouyant, and viscous terms are

the dominant momentum conservation effects. Finally, the GEM algorithm was much more computationally efficient at Rayleigh numbers above 10^4 than MacGregor's program.

The Computation of One-Dimensional Flow with a Large Density Variation

We define a function ϵ_{ij} to be the local error in the conservation of energy due to the compressibility of the fluid

$$\epsilon_{ij} = \dot{P}_a V/(\phi\theta)_{ij}^{n+\delta} - (E/\theta)_{ij}^{n+\delta} - D_{ij}^{n+1},$$

which should be zero. Depending upon the number of iterations used in solving the Poisson's equation for the cell pressure, ϵ_{ij} may deviate from zero. The extent to which ϵ_{ij} persists over the space and in time depends strongly upon the number of iterations used and the compressibility of the fluid. To examine the behavior of the GEM algorithm for strongly compressible fluids, three one-dimensional numerical problems were studied with a fluid whose properties were those of an ideal gas but with $T_0 = 40°\text{R}$.

1. A heating rate at the left boundary was computed which yielded a time rate of change of P_a to be zero with no fluid expulsion. The right boundary was set at a constant lower temperature than the initial temperature.

2. The left and right boundary temperatures were impulsively changed to constant, but different values, and the expulsion rate was chosen to maintain $\dot{P}_a = 0$.

3. No expulsion was permitted and the end temperatures were fixed so that P_a varies in time.

All three studies gave similar results and only those of case 1 are presented.

For problem 1, the fluid moves from the heated to the cooled side subsequent to the application of the heating and cooling at the left and right hand edge, respectively. Initially, the flow field has a rightward spatially constant mass flow rate, and as the time increases the mass flow vanishes leaving a uniform heat flow rate through the stationary gas by conduction.

Figure 5 shows the behavior of the maximum error in the mass flow rate when using the GEM algorithm, with NIP equal to 20. If NIP is fixed at 40, about ten cycles are required before the error assumes a constant value of 0.4 %. Even for NIP = 10, the maximum error diminishes to less than 1 % in about 20 cycles. If NIP is equal to 400, the error in the maximum mass rate is less than 0.1 % for all time.

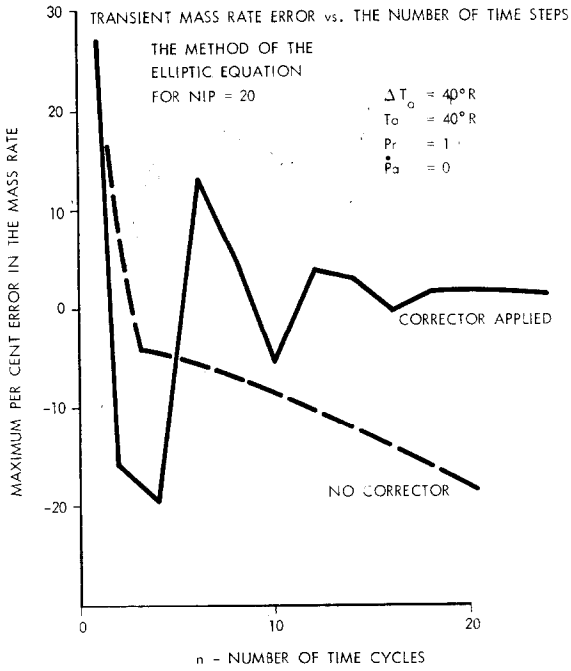

FIG. 5. Maximum error in the mass rate for a compressible fluid in a cavity.

When the GEM algorithm does not contain the compressible fluid corrector, that is, when D_{ij}^n is replaced by $(\dot{P}_a V/\phi\theta)_{ij}^{n+\delta-1} - (E/\theta_{ij}^{n+\delta-1}$, the algorithm does not show the prominent self-correcting tendency which is displayed in Fig. 5, and it was necessary to set NIP = 200 to maintain the maximum value of ϵ_{ij} less than 1 % for all times considered. It should be understood that mass is conserved over the total volume, irrespective of the error in ϵ_{ij}. Thus, the mass in the enclosure as determined by (a) integrating the expulsion rate in time; (b) integrating the mass in the cells; and (c) summing the net expulsion rates of all the cells all differed by less than one place in the fifth significant figure with the IBM 7094 computer. This result is not unexpected since the GEM algorithm algebraically conserves mass.

CAVITY FLOW WITH A LARGE DENSITY VARIATION

The GEM algorithm was applied to the two-dimensional cavity flow problem previously rested for an incompressible fluid with an ideal gas at 20°R and with the hot wall raised to 30°R while the cold wall was maintained at 10°R. The transient

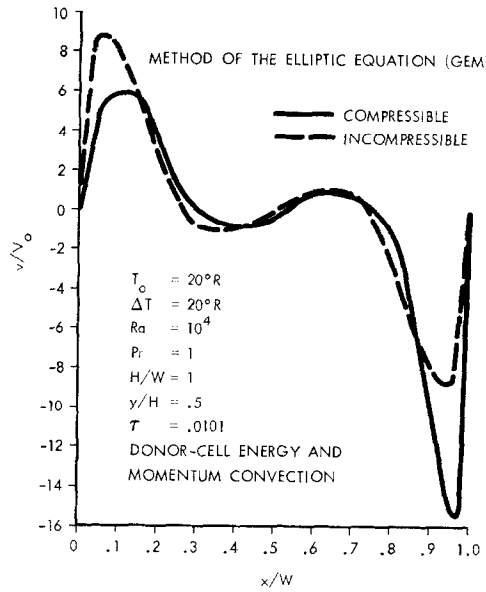

FIG. 6. Compressible fluid transient velocity profile in a cavity.
($V_0 = \mu/\rho/W$)

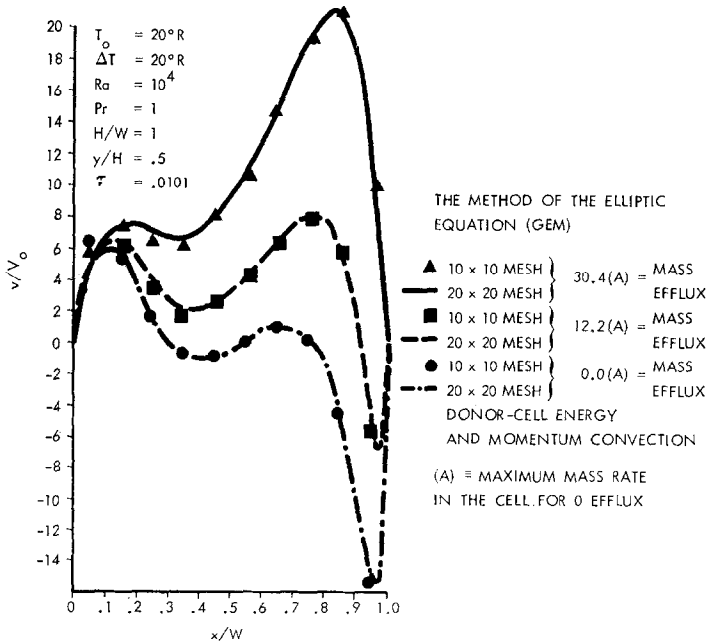

FIG. 7. Compressible fluid transient velocity profile in a cavity from which mass is expelled.
($V_0 = \mu/\rho/W$)

velocity profiles are given in Fig. 6 for the time at which the reverse flow in the region $0.3 \leqslant x/W \leqslant 0.55$ was a maximum. The asymmetry introduced by the variable density is easily observed. During the transient phase the average fluid pressure decayed with time because of a greater heat transfer at the cold wall. At steady state $\dot{P}_a = 0$, irrespective of the grid refinement but the left and right wall Nusselt numbers only approached each other as the grid was refined enough to resolve the asymmetrical boundary layers. Using NIP $= 40$, $\epsilon_{ij\max}$ had decreased to 0.14% after 70 time steps, and with NIP $= 400$, was less than 0.1% after the first time step. Experiments with NIP showed that the method is unstable for any Δt if NIP $= 1$, neutrally stable for NIP $= 2$, and ϵ_{ij} behaves as a damped oscillation for subsequent time cycles if NIP $\geqslant 4$.

The enclosure was also permitted to expel mass at the upper right-hand corner at rates of 5 and 12.5 times the maximum steady state mass flux in the enclosure for the problem of Fig. 3, and some transient velocity profiles are given in Fig. 7. The highest expulsion rate eliminated the reverse flow at the mid-cross section at all times but the free convection flow across the bottom of the enclosure was always present.

Conclusions

For free convection flows where acoustic waves and local variations in compression and expansion are not significant, the energy equation can be adequately expressed in terms of the average fluid pressure rather than the local pressure. By doing so, the time step for the transient computation is not restricted by the acoustic wave speed. Furthermore, it is shown that the Boussinesq assumption is not needed and in fact that it is computationally simpler and faster compared to some incompressible formulations to utilize the primitive variables of P, T, ρ, $\bar{X}$, and $\bar{Y}$ to account for pressure and thermal expansion effects, rather than attempting to make some simplifying assumptions regarding the density effects.

References

1. J. Mihaljan, A rigorous exposition of the Boussinesy approximations applicable to a thin layer of fluid, *Astrophys. J.* **136** (1962), 1126–1131.
2. F. H. Harlow and J. E. Welch, *Phys. Fluids* **8** (1965), 182.
3. W. England and A. F. Emery, Thermal radiation effects on the laminar free convection boundary layer of an absorbing gas, *ASME J. Heat Transfer* Ser. C **91** (1969), 37–45.
4. J. D. Dale and A. F. Emery, The free convection of heat from a vertical plate to several non-Newtonian pseudo plastic fluids, *ASME J. Heat Transfer* Sec. *C* **94** (1972), 64–73.
5. C. K. Forester, Pressurized expulsion of nonisothermal single-phase cryogen, MSC Cryogenic Symposium Papers, NASA Manned Spacecraft Center, Houston, TX, May 20–21, 1971.

6. C. K. FORESTER, Task Summary Report, Math Model Improvement, NASA Manned Spacecraft Center, Houston, TX, July 9, 1971.
7. J. E. FROMM, Practical investigation of convective difference approximation of Reduced Dispersion, *Phys. Fluids Suppl.* **2** (1969), 3–13.
8. C. K. FORESTER, Numerical integration of conservation equations for the storage and expulsion of single-phase cryogens, M. S. Thesis, University of Washington, 1969.
9. G. P. WILLIAMS, *J. Fluid Mech.* **37** (1969), 727.
10. H. Z. BARAKAT, "Finite Difference Computation of Natural Convective Flows in Cylindrical Containers," Ph.D. Thesis, University of Michigan, 1965.
11. C. W. HIRT, Heuristic Stability theory for finite difference equations, *J. Computational Phys.* **2** (1968), 339–355.
12. R. D. RICHTMYER AND R. W. MORTON, "Difference Methods for Initial Value Problems," Interscience, New York, 1967.
13. R. K. MACGREGOR, "The Natural Convection of Fluids in Rectangular Vertical Enclosures," Ph.D. Thesis, University of Washington, 1967.
14. J. O. WILKES, "The Finite Difference Computation of Natural Convection in an Enclosed Rectangular Cavity," Ph.D. Thesis, University of Michigan, 1965.
15. G. DEVAHL DAVIS AND C. F. KETTLEBOROUGH, Natural convection in an enclosed rectangular cavity, *Mech. Chem. Eng.*, **1** (1965), 43–49.
16. S. A. PIACSEK AND G. P. WILLIAMS, Conservation properties of convective difference schemes, *J. Computational Phys.* **6** (1970), 392–905.
17. W. P. CROWLEY, *Monthly Weather Rev.* **96** (1968), 1–15.
18. J. E. FROMM, "A Numerical Method for Computing the Nonlinear, Time-Dependent, Buoyant Circulation of Air in Rooms," IBM Report RJ732 (# 13871) July 28, 1970, IBM Research Laboratory, San Jose, CA.
19. C. K. FORESTER, Prediction of the pressure and temperature fluctuation in the Apollo 12 and 14 oxygen tanks, *Advan. Cryogenic Eng.*, to appear.